Cold season emissions dominate the Arctic tundra methane budget

Donatella Zona[a,b,1,2], Beniamino Gioli[c,2], Róisín Commane[d], Jakob Lindaas[d], Steven C. Wofsy[d], Charles E. Miller[e], Steven J. Dinardo[e], Sigrid Dengel[f], Colm Sweeney[g,h], Anna Karion[g], Rachel Y.-W. Chang[d,i], John M. Henderson[j], Patrick C. Murphy[a], Jordan P. Goodrich[a], Virginie Moreaux[a], Anna Liljedahl[k,l], Jennifer D. Watts[m], John S. Kimball[m], David A. Lipson[a], and Walter C. Oechel[a,n]

[a]Department of Biology, San Diego State University, San Diego, CA 92182; [b]Department of Animal and Plant Sciences, University of Sheffield, Sheffield S10 2TN, United Kingdom; [c]Institute of Biometeorology, National Research Council, Firenze, 50145, Italy; [d]School of Engineering and Applied Sciences, Harvard University, Cambridge, MA 02138; [e]Jet Propulsion Laboratory, California Institute of Technology, Pasadena, CA 91109-8099; [f]Department of Physics, University of Helsinki, FI-00014 Helsinki, Finland; [g]Cooperative Institute for Research in Environmental Sciences, University of Colorado, Boulder, CO 80304; [h]Earth System Research Laboratory, National Oceanic and Atmospheric Administration, Boulder, CO 80305; [i]Department of Physics and Atmospheric Science, Dalhousie University, Halifax, Nova Scotia, Canada B3H 4R2; [j]Atmospheric and Environmental Research, Inc., Lexington, MA 02421; [k]Water and Environmental Research Center, University of Alaska Fairbanks, Fairbanks, AK 99775-7340; [l]International Arctic Research Center, University of Alaska Fairbanks, Fairbanks, AK 99775-7340; [m]Numerical Terradynamic Simulation Group, College of Forestry & Conservation, The University of Montana, Missoula, MT 59812; and [n]Department of Earth, Environment and Ecosystems, Open University, Milton Keynes, MK7 6AA, United Kingdom

Edited by Mark H. Thiemens, University of California at San Diego, La Jolla, CA, and approved November 17, 2015 (received for review August 12, 2015)

Arctic terrestrial ecosystems are major global sources of methane (CH_4); hence, it is important to understand the seasonal and climatic controls on CH_4 emissions from these systems. Here, we report year-round CH_4 emissions from Alaskan Arctic tundra eddy flux sites and regional fluxes derived from aircraft data. We find that emissions during the cold season (September to May) account for ≥50% of the annual CH_4 flux, with the highest emissions from noninundated upland tundra. A major fraction of cold season emissions occur during the "zero curtain" period, when subsurface soil temperatures are poised near 0 °C. The zero curtain may persist longer than the growing season, and CH_4 emissions are enhanced when the duration is extended by a deep thawed layer as can occur with thick snow cover. Regional scale fluxes of CH_4 derived from aircraft data demonstrate the large spatial extent of late season CH_4 emissions. Scaled to the circumpolar Arctic, cold season fluxes from tundra total 12 ± 5 (95% confidence interval) Tg CH_4 y^{-1}, ∼25% of global emissions from extratropical wetlands, or ∼6% of total global wetland methane emissions. The dominance of late-season emissions, sensitivity to soil environmental conditions, and importance of dry tundra are not currently simulated in most global climate models. Because Arctic warming disproportionally impacts the cold season, our results suggest that higher cold-season CH_4 emissions will result from observed and predicted increases in snow thickness, active layer depth, and soil temperature, representing important positive feedbacks on climate warming.

permafrost | aircraft | fall | winter | warming

Emissions of methane (CH_4) from Arctic terrestrial ecosystems could increase dramatically in response to climate change (1–3), a potentially significant positive feedback on climate warming. High latitudes have warmed at a rate almost two times faster than the Northern Hemisphere mean over the past century, with the most intense warming in the colder seasons (4) [up to 4 °C in winter in 30 y (5)]. Poor understanding of controls on CH_4 emissions outside of the summer season (6–10) represents a large source of uncertainty for the Arctic CH_4 budget. Warmer air temperatures and increased snowfall can potentially increase soil temperatures and deepen the seasonal thawed layer, stimulating CH_4 and CO_2 emissions from the vast stores of labile organic matter in the Arctic (11). The overwhelming majority of prior studies of CH_4 fluxes in the Arctic have been carried out during the summer months (12–15). However, the fall, winter, and spring months represent 70–80% of the year in the Arctic and have been shown to have significant emissions of CO_2 (16–18). The few measurements of CH_4 fluxes in the Arctic that extend into the fall (6, 7, 9, 10) show complex patterns of CH_4 emissions, with a number indicating high fluxes (7, 10). Winter and early spring data appear to be absent in Arctic tundra over continuous permafrost.

Beginning usually in late August or early September, the seasonally thawed active layer (i.e., ∼30–50 cm, near-surface soil layer over the permafrost that thaws during the summer growing season) in the Arctic starts freezing both from the top and the bottom, moving downward from the frozen, often snow-covered soil surface and upward from the permafrost layer (Fig. 1). A significant portion of the active layer can stay unfrozen for months, with temperatures poised near 0 °C because of the large thermal mass and latent heat of fusion of water in wet soils, and for the insulating effects of snow cover and low density surface

Significance

Arctic ecosystems are major global sources of methane. We report that emissions during the cold season (September to May) contribute ≥50% of annual sources of methane from Alaskan tundra, based on fluxes obtained from eddy covariance sites and from regional fluxes calculated from aircraft data. The largest emissions were observed at the driest site (<5% inundation). Emissions of methane in the cold season are linked to the extended "zero curtain" period, where soil temperatures are poised near 0 °C, indicating that total emissions are very sensitive to soil climate and related factors, such as snow depth. The dominance of late season emissions, sensitivity to soil conditions, and importance of dry tundra are not currently simulated in most global climate models.

Author contributions: D.Z., D.A.L., and W.C.O. designed research; D.Z., D.A.L., and W.C.O. performed research; R.C., J.L., S.C.W., C.E.M., S.J.D., C.S., A.K., R.Y.-W.C., and J.M.H. supported the collection and preparation of the Carbon in Arctic Reservoirs Vulnerability Experiment data; J.D.W. and J.S.K. contributed new reagents/analytic tools; D.Z., B.G., P.C.M., J.P.G., V.M., A.L., J.D.W., J.S.K., and W.C.O. analyzed data; R.C., J.L, and S.C.W. analyzed the aircraft data; and D.Z., B.G., R.C., S.C.W., C.E.M., S.J.D., S.D., C.S., A.K., R.Y.-W.C., J.M.H., P.C.M., A.L., J.D.W., J.S.K., D.A.L., and W.C.O. wrote the paper.

The authors declare no conflict of interest.

This article is a PNAS Direct Submission.

Freely available online through the PNAS open access option.

Data deposition: The data reported in this paper have been deposited in the Oak Ridge National Laboratory Distributed Active Archive Center, Oak Ridge data repository (dx.doi.org/10.3334/ORNLDAAC/1300 and dx.doi.org/10.3334/CDIAC/hippo_010).

[1]To whom correspondence should be addressed. Email: dzona@mail.sdsu.edu.

[2]D.Z. and B.G. contributed equally to this work.

This article contains supporting information online at www.pnas.org/lookup/suppl/doi:10.1073/pnas.1516017113/-/DCSupplemental.

Downloaded from https://www.pnas.org by 72.197.169.76 on April 1, 2022 from IP address 72.197.169.76.

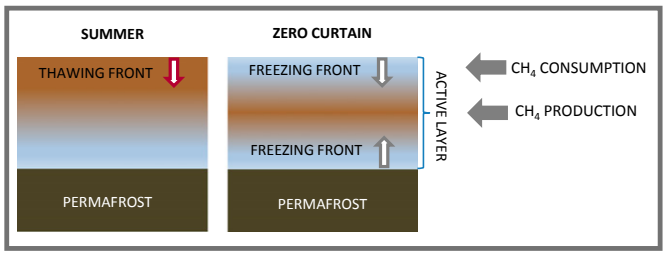

Fig. 1. Diagram of the hypothesized soil physical processes influencing CH_4 production and oxidation depending on the time of the season. We expect that during the zero curtain, the frozen near surface soil layer decreases CH_4 oxidation, resulting in substantial CH_4 emissions, even with lower CH_4 production. Light blue represents cooler soil temperatures, and light brown represents warmer soil temperatures; the arrows point in the direction of the thawing fronts in the summer and freezing front during the cold period.

material. This period has been denoted as the "zero curtain" (19). Soil freezing toward the end of the zero curtain period was considered responsible for sporadic peaks in CH_4 emissions observed in the fall (7, 10), but very sparse data are available to evaluate the importance of fall emissions over a larger scale. The processes influencing CH_4 production and emission in tundra during the cold period (Fig. 1) are not fully explored or understood.

In this paper, we present, to our knowledge, the first year-round eddy flux observations for CH_4 in the Arctic tundra over continuous permafrost to address the critical knowledge gap in cold season CH_4 emissions. Data were obtained from five eddy covariance (EC) towers along a 300-km latitudinal transect on the North Slope of Alaska, with sites extending south from Barrow [Barrow Environmental Observatory (BEO) tower; Biocomplexity Experiment, South (BES) tower; Climate Monitoring and Diagnostics Laboratory (CMDL) tower] to Atqasuk (ATQ) and Ivotuk (IVO) (Fig. 2 and *Materials and Methods*), spanning from June 2013 to January 2015 to capture two summer–fall–winter cycles. We investigated the spatial representativeness of the EC tower data at the regional scale by comparing to CH_4 fluxes estimated from analysis of 15 aircraft flights over the North Slope (2012 to 2014), part of National Aeronautics and Space Administration's Carbon in Arctic Vulnerability Experiment (CARVE). We also examined the correlation between CH_4 concentrations and CO from the High-performance Instrumented Airborne Platform for Environmental Research (HIAPER) Pole-to-Pole Observation (HIPPO) global-scale measurement program to assess whether biological emissions during the cold season measurably influence global distributions of atmospheric CH_4.

Results and Discussion

Site-Level CH_4 Fluxes. Fig. 2 shows continuous eddy flux data for five tundra sites in Alaska: three in Barrow (CMDL, BEO, and BES), one in ATQ, and one in IVO (*Materials and Methods*). Methane emission rates from the cold seasons (September to May) were comparable to (e.g., BEO and ATQ; Fig. 1 *C* and *D*) or higher than (e.g., CMDL; Fig. 1*B*) emissions in summer over a prolonged period. Cumulative emissions for the cold season

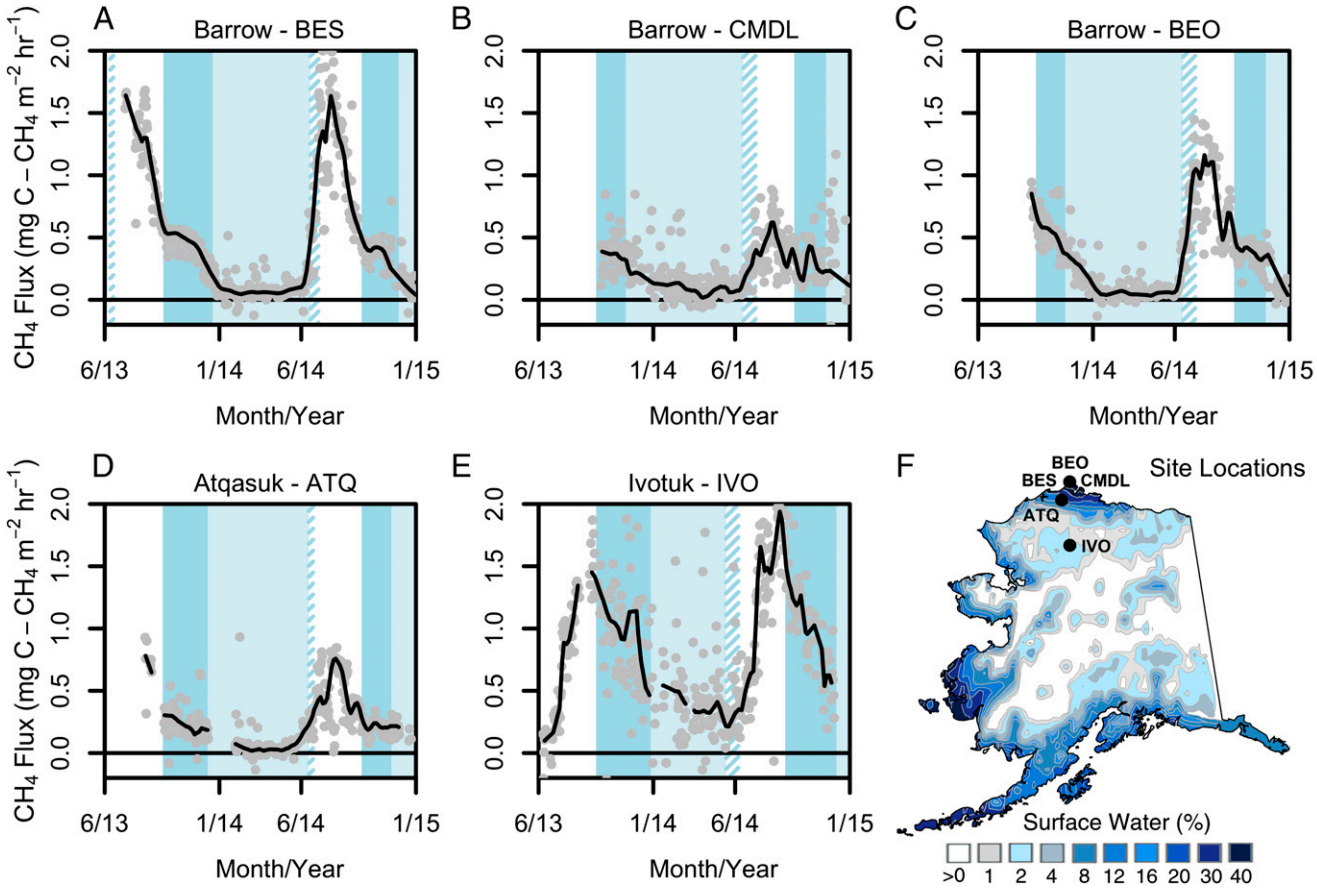

Fig. 2. Methane flux (mg C-CH_4 m^{-2} h^{-1}) measured at the five EC sites on the North Slope, AK: Barrow-BES (*A*), Barrow-BEO (*B*), Barrow-CMDL (*C*), ATQ (*D*), and IVO (*E*) from June 2013 to January 2015 [the gray dots are daily median for a minimum of 24 points per day, and the black line is a 35-d smoothing (lowess) applied to that daily median]. (*F*) Map of Alaska indicating the location of the sites and the percentage of surface inundation (*SI Materials and Methods*). The zero curtain (dark blue), spring thawing with soil temperature around 0 ± 0.75 °C (diagonal hatching) (Fig. S1 and Table S1), summer (no shading), and the balance of the cold season below −0.75 °C (light blue) periods are indicated (*A*–*E*).

Downloaded from https://www.pnas.org by 72.197.169.76 on April 1, 2022 from IP address 72.197.169.76.

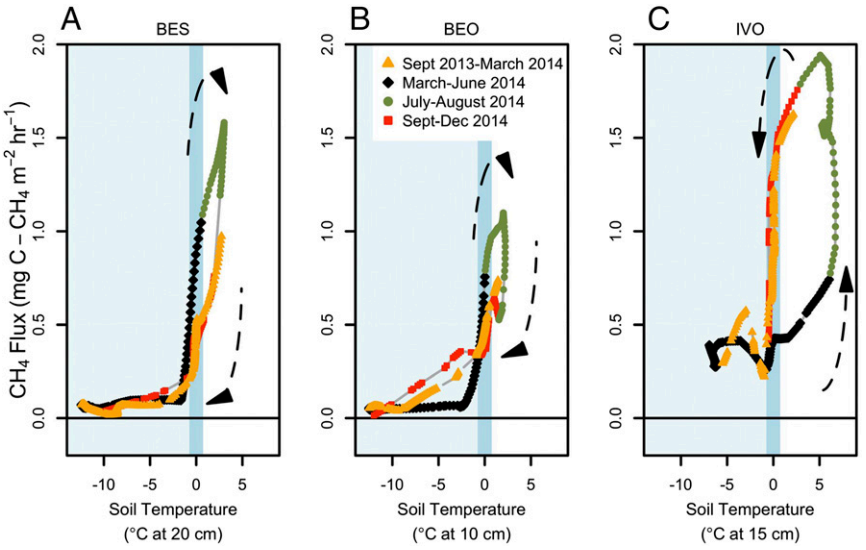

Fig. 3. The methane flux variation with soil temperature on the North Slope of Alaska at Barrow-BES (BES) (*A*), Barrow-BEO (BEO) (*B*), and IVO (*C*) during the indicated periods. The zero curtain period is shaded in dark blue, with soil temperatures below −0.75 °C in lighter blue. The seasonal progression of each phase is indicated by the black arrows. Winter-time data are shown as orange triangles (September 1, 2013 to March 12, 2014) and red squares (September 1, 2014 to December 31, 2014). Data collected during the spring (March 13, 2014 to June, 30, 2014) are shown as black diamonds. Data during the summer period (July 1, 2014 to August 31, 2014) are shown as green circles.

averaged 1.7 ± 0.2 [mean ± confidence interval (CI)] g C-CH_4 m^{-2} at our five sites, accounting on average for 50 ± 9% (mean ± CI) of the annual budget (BES, 37%; BEO, 43%; CMDL, 64%; ATQ, 47%; IVO, 59%). Cold-season emissions dominated the annual CH_4 budget in the driest sites (CMDL, ATQ, IVO), representing a notably higher contribution than previously modeled (6) in other continuous permafrost sites (35%) and also higher than observed year round in boreal Alaska [40%, using periodic sampling of static chambers (20)]. The boreal systems are underlain by discontinuous or sporadic permafrost and are therefore subject to different soil processes than Arctic sites underlain by continuous permafrost (which prevents drainage for extended areas for example).

The highest fall and winter CH_4 fluxes were observed at IVO, an upland tundra site (with a water table below the surface for most of the summer), which had the longest zero curtain period (101 d; Table S1), the warmest soil temperatures during the cold season (Fig. 3 and Fig. S1), the deepest snow depth (*SI Materials and Methods*), and the deepest active layer (Fig. S2 *A* and *B*). Soil temperatures were also poised near 0 °C for more than 90 d at much wetter sites near Barrow (BES). In both cases, the zero curtain period lasted as long as, or longer than, the summer season (Fig. S1 and Table S1). Based on direct measurement of the active layer depth and on soil temperature data, the maximum thaw depth did not begin to decrease appreciably until November or later in all of the sites measured (Fig. S2 *A* and *B*), even though the surface froze in September. During the zero curtain period, we observed strong CH_4 emissions from all five sites, 0.3–2.4 g C-CH_4 m^{-2} (Fig. 2), albeit somewhat lower than the peak summer season CH_4 fluxes observed. The overall contribution of these zero curtain periods to annual emissions was important because of their extended duration (Fig. 2, Fig. S1, and Table S1): emissions of CH_4 during the zero curtain period alone contributed ∼20% of the annual budget (BES, 18%; BEO, 20%; CMDL, 20%; ATQ, 16%; IVO, 32%).

A few previous studies reported measurements of Arctic CH_4 fluxes during the fall (6, 7, 9, 10), but the measurements did not extend to winter and spring. We found that sites with similar summertime CH_4 fluxes had different zero curtain emissions because of different durations and depths of unfrozen soil (Fig. 2 and Fig. S2). For example, summertime cumulative emissions in IVO were 1.9 g C-CH_4 m^{-2} in 2013 and 2.7 g C-CH_4 m^{-2} in 2014, similar to the 2.3 g C-CH_4 m^{-2} (in both years) at BES. However, cumulative CH_4 emissions during the zero curtain were much higher in IVO (2.4 and 2.1 g C-CH_4 m^{-2} in 2013 and 2014, respectively) than BES (0.9 and 0.7 g C-CH_4 m^{-2} in 2013 and 2014, respectively) probably because of interacting effects of greater CH_4 production at IVO, the inhibition of surface oxidation in the fall (Fig. 1), and the deeper thaw depth delaying the complete soil freezing in IVO (Figs. S1 and S2). The emissions of CH_4 produced deeper in the soil continued during the cold season, presumably through cracks and pathways in the near-surface frozen soils (7).

Linear mixed effects modeling (*SI Materials and Methods*) suggested that the depth of the active layer was a critical control on CH_4 fluxes during the summer. The presence of this unfrozen soil layer in the fall and early winter was also a major control on cold season CH_4 emissions; warmer soils resulted in greater CH_4 emission over the entire year. The importance of warm soil temperatures and deep active layer is consistent with the observed higher winter emissions in IVO, where soil temperature at 15 and 30 cm below the surface never dropped below approximately −8 °C compared with at or below −15 °C at the northern sites (e.g., BES and ATQ). The observed CH_4 emissions during fall and winter are consistent with data showing significant microbial populations and metabolic activity at and below 0 °C in the Arctic (16, 21), reflecting the availability of unfrozen water films (22) under these conditions (16). Measurable metabolism has been observed down to −40 °C (23), and CH_4 production has been observed down to −16 °C (21, 24). Soil particles maintain liquid water films until a temperature of at least −10 °C (25), and this unfrozen water can sustain microbial metabolism and greenhouse gas production (26), even as the soil bulk water freezes (25). The direct effect of higher temperature on metabolic activity and the indirect effect of temperature through greater liquid water volume should result in a larger population size and more activity in the methanogenic (i.e., methane-producing) community in the winter at IVO compared with the other, colder, sites. Unfortunately, IVO is the only tower collecting CH_4 fluxes and environmental variables continuously year round over upland tundra at this latitude in Alaska. Therefore, we encourage the establishment of similar upland sites in the Arctic to confirm these observations.

Across all our sites, areas of lower inundation (i.e., less surface area with water table above the surface for most or all of the growing season) had the greatest percentage of total emissions from the cold season, with the highest emissions from IVO with <5% inundation (Fig. 2). In contrast, most modeling studies limit CH_4 emissions to areas with inundated or saturated soils (27). The observed CH_4 emissions that persisted, even when temperatures were well below 0 °C (Fig. 2), present a remarkably

Downloaded from https://www.pnas.org by 72.197.169.76 on April 1, 2022 from IP address 72.197.169.76.

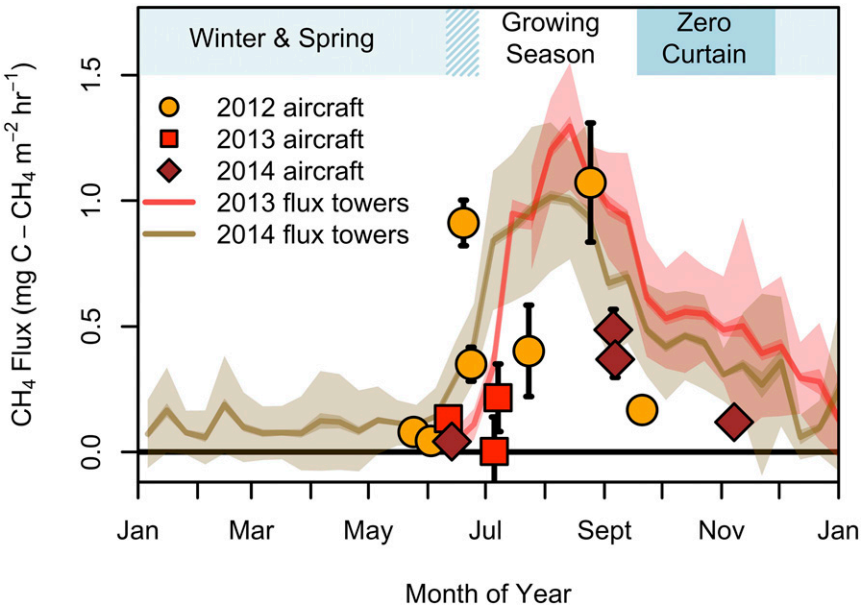

Fig. 4. Ten-day block average of the five EC flux towers over a 300-km transect across the North Slope of Alaska (shaded bands) for 2013 (red) and 2014 (brown), with the mean (solid line), 95% confidence intervals (darker shade), and SD in the CH_4 data (lightest shade). The regional fluxes of CH_4 calculated from the CARVE aircraft data for the North Slope of Alaska are shown for 2012 (yellow circles), 2013 (red squares), and 2014 (brown diamonds). The mean dates for the onset of winter, the growing season, and the zero curtain are indicated in the band on top. Regional scale fluxes of CH_4 (mg C-CH_4 m^{-2} h^{-1}) showed similar seasonal pattern to the EC flux towers across multiple years.

uniform temperature response with a decrease in emission rates as soil temperatures drop (Fig. 3). The fall fluxes show clear relationships with declining soil temperature in the active layer, with little discontinuity in the flux relationship with soil temperature as the soils freeze (Fig. 3). It is likely that freezing of the surface soils decreases near-surface CH_4 oxidation (Fig. 1), maintaining net soil CH_4 emissions even as decreasing soil temperatures results in decreasing CH_4 production rates. At IVO, warmer soil and deeper thaw depth (and therefore greater metabolically active soil volume) resulted in the highest cold season emission rates. This seasonal pattern is very different from that reported by Mastepanov et al. (7, 10), who showed a drop in emissions in late summer/early fall from Greenland tundra, followed by large late-fall CH_4 emissions peaking during complete freezing of the active layer. We instead found fall emissions were persistent until the soil temperatures were well below 0 °C (Fig. 2), with a few instances of sporadic, exceptionally high emissions, e.g., in IVO (Fig. 2) contributing just ∼15% of the zero curtain emissions and ∼5% of the total annual CH_4 emissions. The underlying sensitivity of CH_4 fluxes to temperature at our sites was, on average, a factor of 2.7 (Fig. 2) for a temperature rise from 0°, to 5 °C, slightly more sensitive than the global mean described by Yvon-Durocher et al. (2).

Spring CH_4 fluxes also increased with increasing active layer temperatures (Fig. 3). The northern sites (e.g., BES and BEO; Fig. 3) showed prompt, steep increases in CH_4 emissions coincident with increasing soil temperatures. The southernmost site (IVO) showed a very different pattern, with apparently much lower temperature sensitivity of net fluxes in the spring vs. fall (Fig. 3). Unlike the wet tundra sites, there is substantial seasonal hysteresis at IVO, likely reflecting a combination of CH_4 oxidation in the spring and summer in the warmer, dry surface layers and CH_4 storage in the deepening, porous active layer. Also, methanogenesis may be stimulated by reduced oxygen in the unfrozen active layer, because the frozen surface (Fig. 1) slows diffusion of oxygen into the soil column (28).

Microbial consumption of CH_4 in the near-surface soil layer (methanotrophy) can be very active in summer (28) but is inhibited by near-surface soil freezing (28, 29). Thus, the fraction of CH_4 escaping to the atmosphere likely increases as the soil surface freezes in the fall. The wettest sites, such as Barrow-BES, where the water table was on average above the surface for the entire measuring period (Fig. S2 *C* and *D*), presumably had low levels of surface oxidation of CH_4. Therefore, this site showed the greatest relative decrease of cold season CH_4 fluxes compared with summer (Fig. 2) because decreasing temperatures reduced CH_4 production, but because oxidation rates were low, there was little benefit from suppression of oxidation in the surface layer in fall.

Our measurements of CH_4 emissions from Arctic tundra are more extensive in both time and space than what have been used to develop and test existing models. Annual CH_4 emissions rates from noninundated Arctic tundra (<20% surface water; Fig. 2) are comparable to those of inundated environments. Most models map CH_4 fluxes to the Arctic landscape using inundation (27), thus dramatically underestimating the emitting area in the Arctic, including during the cold season. The zero curtain interval in fall and winter, and even the period of frozen soils in winter, produce significant, previously underestimated, CH_4 emissions (27). Our work provides the basis for parametric representation of these fluxes and highlights the critical importance of driving models with subsurface soil temperature, and not air temperature.

Regional and Global Scale CH_4 Estimates. Regional CH_4 fluxes calculated from aircraft observations (30) show a strikingly consistent pattern to our eddy flux data (Fig. 4), notably including the persistence of CH_4 emissions into the cold season. The regional aircraft fluxes derived from the CARVE (*Materials and Methods*, *SI Materials and Methods*, and Fig. S3) flights were at times lower than the mean of the EC tower fluxes, as has been observed previously in point-scale and regional-scale flux comparisons (*SI Materials and Methods*). Global-scale measurements (HIPPO; *Materials and Methods*) detected a large enhancement of CH_4 in the Arctic in early November, peaking in the boundary layer of the northern high latitudes (Fig. 5). Because of the flight plans of the HIPPO flights conducted in 2009 to 2011, fluxes

Downloaded from https://www.pnas.org by 72.197.169.76 on April 1, 2022 from IP address 72.197.169.76.

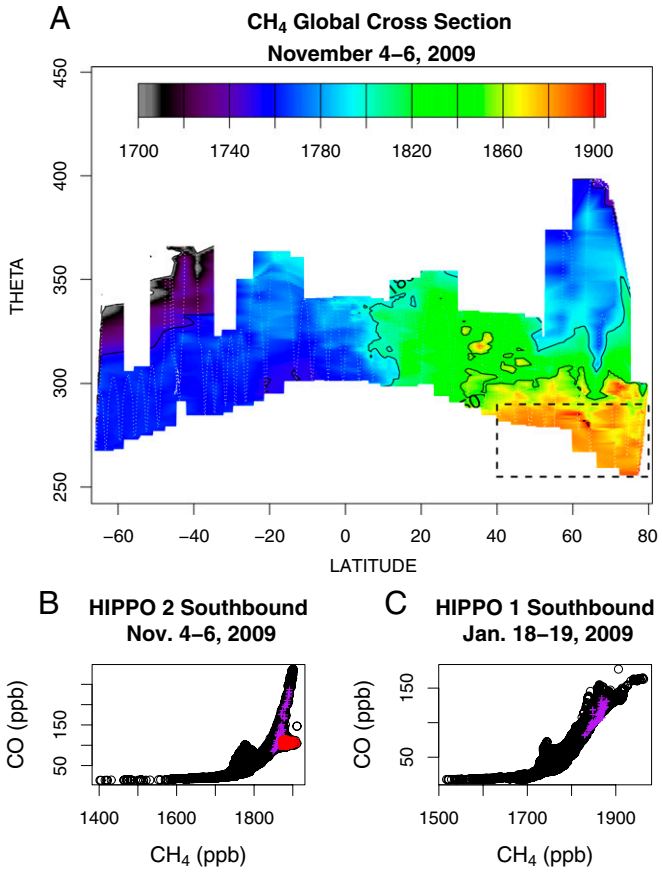

Fig. 5. (*A*) Global cross-section of HIPPO data for CH_4 in the central Pacific and across Alaska (November 4–10, 2009) plotted with potential temperature as the vertical coordinate. The highest CH_4 concentrations are at middle and high latitudes, including the cold, dense air of the high Arctic. (*B*) Methane plotted against CO for the flight data of November 4–10, 2009, showing a subfamily of red points with elevated CH_4 but no corresponding enhancement of CO. (*C*) Same as in *B* but for January 18–25, 2009. In contrast to the November data, elevated CH_4 values are consistently associated with corresponding elevated CO values in January. These results show that elevated CH_4 in November is not associated with anthropogenic CO.

could not be calculated from the HIPPO data. However, the HIPPO data are important to understanding whether the CH_4 fluxes calculated at the flux towers and during CARVE are relevant to CH_4-mixing ratios on the global scale. In the North Slope vicinity (71° N > latitude >65° N), CH_4 is enhanced compared with the global mean, but there is no corresponding elevation of CO, indicating that the CH_4 sources are not associated with transported pollution or fossil fuel burning (Fig. 5*B*; we have only considered CH_4 data between 65° N and 71° N to remove the influence of CH_4 enhancements observed over open leads in sea ice (32)]. By contrast, in January, there were air parcels with high CH_4 consistently associated with CO enhancement, indicating a dominant anthropogenic source of CH_4 compared with the global mean. During this time CH_4 was likely transported from lower latitudes (31). Overall, the HIPPO data are consistent with a substantial biogenic CH_4 source over northern Alaska in fall and with our finding of strong late season biogenic emissions on both a local and regional spatial scale.

Recent estimates using inverse modeling of atmospheric concentration data give CH_4 emissions from Arctic tundra wetlands in the range from 16 ± 5 Tg CH_4 y^{-1} [from CarbonTracker (32)] to 27 (−15 to 68) Tg CH_4 y^{-1} (8). Extrapolating our average CH_4 emissions rates to the Circumpolar Arctic tundra (*SI Materials and Methods*) yields an estimate of 23 ± 8 Tg CH_4 y^{-1} from Arctic tundra, similar to these previous estimates (8, 32). Our estimated CH_4 cold-season emissions as well as those from inverse analysis (27, 32) are significantly higher than that estimated by land-surface models (27, 32). This difference was thought to be linked to anthropogenic emissions, because biogenic emissions were assumed to be negligible during the cold season (27, 32). Overall, the seasonal patterns estimated by models (27) are very different from ours and generally do not include the substantial cold season CH_4 emissions found here. Our finding of large cold-season biogenic emissions from tundra reconciles the atmospheric observations and inverse model estimates without the need to invoke a large pollution influence.

Conclusions

Continued warming and deeper snow are forecast for the future in the Arctic (33). Our results indicate these changes will result in globally significant increases in CH_4 emissions and that cold-season emissions will become increasingly important in this process. Additional year-round CH_4 fluxes and soil climate measurements at sites across the Arctic are urgently needed.

Our results contradict model predictions that simulate and predict the largest CH_4 emissions from inundated landscape. We showed that the largest CH_4 emissions are actually from the site with very low inundation. We believe that the results of our study will impinge directly on our ability to predict future Arctic CH_4 budgets and allow us to revise the variables and processes that must be included to capture the true sensitivity of Arctic CH_4 emissions to climate change.

Materials and Methods

Ecosystem-scale CO_2 and CH_4 fluxes were measured using the EC method with three EC towers in Barrow (9, 15, 34) (CMDL) (71.3225269 N, −156.6091798 W), BEO (71.2810016 N, −156.6123454 W), and BES (71.280881 N, −156.596467 W); one EC tower in ATQ (18) (70.4696228 N, −157.4089471 W); and one EC tower in IVO (68.48649 N, −155.75022 N). The EC towers in CMDL, BEO, BES, and ATQ were upgraded during the summer and fall of 2013 to include closed-path Los Gatos Research (LGR) analyzers [Fast Greenhouse Gas Analyzer (FGGA); LI-7200 (LICOR) (CMDL, ATQ, and IVO); LI-7700 (in IVO in April 2013 and at CMDL in June 2011); a uSonic-3 Class-A (METEK) sonic anemometer (ATQ and IVO); and CSAT-3D (Campbell Scientific) sonic anemometer (BEO, BES, ATQ, and IVO)] which were installed in summer and fall 2013. Fig. S3 displays the regional scale footprint estimates and fluxes from CARVE, Fig. S4 displays the data coverage of the EC CH_4 fluxes for each of the sites, and Fig. S5 displays the comparison between the LI-7700 and LGR. Gap filling of the CH_4 flux data are described in *SI Materials and Methods*, Figs. S6 and S7, and Table S2. To indicate the sites in this study, we used similar names to the ones used in AmeriFlux for ATQ (AmeriFlux site name, US-Atq), for IVO (AmeriFlux site name, US-Ivo), and for BES (AmeriFlux site name, US-Bes) not for Barrow-CMDL (US-Brw) because three sites in Barrow are included in this analysis.

The global-scale measurements were made as part of the HIPPO of Carbon Cycle and Greenhouse Gases Study, flown aboard the National Center for Atmospheric Research (NCAR)-operated HIAPER aircraft. Transects spanned the Pacific from 85° N to 67° S, with vertical profiles every ~2.2° of latitude during five separate deployments during 2009 to 2011, covering all seasons (35). CH_4-mixing ratios were measured using a midinfrared quantum cascade laser spectrometer (QCLS), developed by Harvard University and Aerodyne Research and operated during HIPPO by the same Harvard team that measured CH_4 during CARVE (30, 36). Common calibration procedures and National Oceanic and Atmospheric Administration (NOAA)-calibrated standards were used during both HIPPO and CARVE, allowing for direct comparison of CH_4-mixing ratios.

ACKNOWLEDGMENTS. We thank the Global Change Research Group at San Diego State University, UMIAQ, Ukpeagvik Inupiat Corporation (UIC), CH2M HILL Polar Services for logistical support; Salvatore Losacco, Owen Hayman, and Herbert Njuabe for help with field data collection; David Beerling for comments on the manuscript; Scot Miller for suggestions on the statistical analysis; and George Burba for suggestions on the data quality assessment. The statistical analysis was performed using R, and we thank the R Developing Core Team. This research was conducted on land owned by the UIC. This

Downloaded from https://www.pnas.org by 72.197.169.76 on April 1, 2022 from IP address 72.197.169.76.

work was funded by the Division of Polar Programs of the National Science Foundation (NSF) (Award 1204263); Carbon in Arctic Reservoirs Vulnerability Experiment (CARVE), an Earth Ventures (EV-1) investigation, under contract with the National Aeronautics and Space Administration; and Department of Energy (DOE) Grant DE-SC005160. Logistical support was funded by the NSF Division of Polar Programs.

1. Kirschke S, et al. (2013) Three decades of global methane sources and sinks. *Nat Geosci* 6(10):813–823.
2. Yvon-Durocher G, et al. (2014) Methane fluxes show consistent temperature dependence across microbial to ecosystem scales. *Nature* 507(7493):488–491.
3. Schuur EAG, et al. (2015) Climate change and the permafrost carbon feedback. *Nature* 520(7546):171–179.
4. Bekryaev RV, Polyakov IV, Alexeev VA (2010) Role of polar amplification in long-term surface air temperature variations and modern Arctic warming. *J Clim* 23(14):3888–3906.
5. Fraser R, Lantz T, Olthof I, Kokelj S, Sims R (2014) Warming-induced shrub expansion and lichen decline in the Western Canadian Arctic. *Ecosystems (N Y)* 17(7):1151–1168.
6. Wille C, Kutzbach L, Sachs T, Wagner D, Pfeiffer E-M (2008) Methane emission from Siberian arctic polygonal tundra: Eddy covariance measurements and modeling. *Glob Change Biol* 14(6):1395–1408.
7. Mastepanov M, et al. (2008) Large tundra methane burst during onset of freezing. *Nature* 456(7222):628–630.
8. McGuire AD, et al. (2012) An assessment of the carbon balance of Arctic tundra: Comparisons among observations, process models, and atmospheric inversions. *Biogeosciences* 9(8):3185–3204.
9. Sturtevant CS, Oechel WC, Zona D, Kim Y, Emerson CE (2012) Soil moisture control over fall season methane flux, Arctic Coastal Plain of Alaska. *Biogeosciences* 9(4):1423–1440.
10. Mastepanov M, et al. (2013) Revisiting factors controlling methane emissions from high-Arctic tundra. *Biogeosciences* 10(11):5139–5158.
11. Hugelius G, et al. (2014) Estimated stocks of circumpolar permafrost carbon with quantified uncertainty ranges and identified data gaps. *Biogeosciences* 11(23):6573–6593.
12. Vourlitis GL, Oechel WC, Hastings SJ, Jenkins MA (1993) A System for Measuring in situ CO_2 and CH_4 Flux in Unmanaged Ecosystems: An Arctic example. *Funct Ecol* 7(3): 369–379.
13. Sachs T, Wille C, Boike J, Kutzbach L (2008) Environmental controls on ecosystem-scale CH_4 emission from polygonal tundra in the Lena River Delta, Siberia. *J Geophys Res Biogeosci* 113(G3):G00A03.
14. Parmentier FJW, et al. (2011) Spatial and temporal dynamics in eddy covariance observations of methane fluxes at a tundra site in northeastern Siberia. *J Geophys Res Biogeosci* 116(G3):G03016.
15. Zona D, et al. (2009) Methane fluxes during the initiation of a large-scale water table manipulation experiment in the Alaskan Arctic tundra. *Global Biogeochem Cycles* 23: GB2013.
16. Monson RK, et al. (2006) Winter forest soil respiration controlled by climate and microbial community composition. *Nature* 439(7077):711–714.
17. Euskirchen ES, Bret-Harte MS, Scott GJ, Edgar C, Shaver GR (2012) Seasonal patterns of carbon dioxide and water fluxes in three representative tundra ecosystems in northern Alaska. *Ecosphere* 3(1):art4.
18. Oechel WC, Laskowski CA, Burba G, Gioli B, Kalhori AAM (2014) Annual patterns and budget of CO_2 flux in an Alaskan arctic tussock tundra ecosystem at Atqasuk, Alaska. *J Geophys Res* 119(3):323–339.
19. Hinkel KM, Paetzold F, Nelson FE, Bockheim JG (2001) Patterns of soil temperature and moisture in the active layer and upper permafrost at Barrow, Alaska: 1993-1999. *Global Planet Change* 29(3–4):293–309.
20. Whalen SC, Reeburgh WS (1988) A methane flux time series for tundra environments. *Global Biogeochem Cycles* 2(4):399–409.
21. Panikov NS, Dedysh SN (2000) Cold season CH_4 and CO_2 emission from boreal peat bogs (West Siberia): Winter fluxes and thaw activation dynamics. *Global Biogeochem Cycles* 14(4):1071–1080.
22. Ostroumov VE, Siegert C (1996) Exobiological aspects of mass transfer in microzones of permafrost deposits. *Adv Space Res* 18(12):79–86.
23. Price PB, Sowers T (2004) Temperature dependence of metabolic rates for microbial growth, maintenance, and survival. *Proc Natl Acad Sci USA* 101(13):4631–4636.
24. Rivkina E, et al. (2004) Microbial life in permafrost. *Adv Space Res* 33(8):1215–1221.
25. Romanovsky VE, Osterkamp TE (2000) Effects of unfrozen water on heat and mass transport processes in the active layer and permafrost. *Permafrost Periglac* 11(3): 219–239.
26. Clein JS, Schimel JP (1995) Microbial activity of tundra and taiga soils at sub-zero temperatures. *Soil Biol Biochem* 27(9):1231–1234.
27. Bohn TJ, et al. (2015) WETCHIMP-WSL: Intercomparison of wetland methane emissions models over West Siberia. *Biogeosciences* 12(11):3321–3349.
28. Yu J, et al. (2007) Enhanced net formations of nitrous oxide and methane underneath the frozen soil in Sanjiang wetland, northeastern China. *J Geophys Res* 112:D07111.
29. Wu X, et al. (2010) Effects of soil moisture and temperature on CO_2 and CH_4 soil atmosphere exchange of various land use/cover types in a semi-arid grassland in Inner Mongolia, China. *Soil Biol Biochem* 42(5):773–787.
30. Chang RY-W, et al. (2014) Methane emissions from Alaska in 2012 from CARVE airborne observations. *Proc Natl Acad Sci USA* 111(47):16694–16699.
31. Sweeney C, et al. (2015) Seasonal climatology of CO2 across North America from aircraft measurements in the NOAA/ESRL Global Greenhouse Gas Reference Network. *J Geophys Res Atmos* 120(10):5155–5190.
32. Bruhwiler L, et al. (2014) CarbonTracker-CH_4: An assimilation system for estimating emissions of atmospheric methane. *Atmos Chem Phys* 14(16):8269–8293.
33. Hay LE, McCabe GJ (2010) Hydrologic effects of climate change in the Yukon River Basin. *Clim Change* 100(3–4):509–523.
34. Zona D, et al. (2012) Increased CO_2 loss from vegetated drained lake tundra ecosystems due to flooding. *Global Biogeochem Cycles* 26(2):GB2004.
35. Wofsy SC (2011) HIAPER Pole-to-Pole Observations (HIPPO): Fine grained, global scale measurements for determining rates for transport, surface emissions, and removal of climatically important atmospheric gases and aerosols. *Philos Trans R Soc Lond A* 369(1943):2073–2086.
36. Kort EA, et al. (2012) Atmospheric observations of Arctic Ocean methane emissions up to 82° north. *Nat Geosci* 5:318–321.
37. Zona D, et al. (2014) Delayed responses of an Arctic ecosystem to an extremely dry summer: Impacts on net ecosystem exchange and vegetation functioning. *Biogeosciences* 11(20):5877–5888.
38. Walker DA, et al. (2005) The Circumpolar Arctic vegetation map. *J Veg Sci* 16(3): 267–282.
39. Vickers D, Mahrt L (1997) Quality control and flux sampling problems for tower and aircraft data. *J Atmos Ocean Technol* 14(3):512–526.
40. Gash JHC, Culf AD (1996) Applying a linear detrend to eddy correlation data in realtime. *Boundary Layer Meteorol* 79(3):301–306.
41. Wilczak J, Oncley S, Stage S (2001) Sonic anemometer tilt correction algorithms. *Boundary Layer Meteorol* 99:127–150.
42. Moncrieff JB, Clement R, Finnigan J, Meyers T (2004) Averaging, detrending and filtering of eddy covariance time series. *Handbook of Micrometeorology: A Guide for Surface Flux Measurements*, eds Lee X, Massman WJ, Law BE (Kluwer, Dordrecht, The Netherlands), pp 7–31.
43. Moncrieff JB, et al. (1997) A system to measure surface fluxes of momentum, sensible heat, water vapour and carbon dioxide. *J Hydrol (Amst)* 188–189:589–611.
44. Ibrom A, Dellwik E, Larsen SE, Pilegaard KIM (2007) On the use of the Webb–Pearman–Leuning theory for closed-path eddy correlation measurements. *Tellus B Chem Phys Meterol* 59(5):937–946.
45. Burba G, et al. (2012) Calculating CO_2 and H_2O eddy covariance fluxes from an enclosed gas analyzer using an instantaneous mixing ratio. *Glob Change Biol* 18(1): 385–399.
46. McDermitt D, et al. (2011) A new low-power, open-path instrument for measuring methane flux by eddy covariance. *Appl Phys B* 102(2):391–405.
47. Horst TW, Lenschow DH (2009) Attenuation of scalar fluxes measured with spatially-displaced sensors. *Boundary Layer Meteorol* 130(2):275–300.
48. Foken T, et al. (2004) Post-field quality control. *Handbook of Micrometeorology: A Guide for Surface Flux Measurements* (Kluwer, Dordrecht, The Netherlands), pp 81–108.
49. Mauder M, Foken T (2006) Impact of post-field data processing on eddy covariance flux estimates and energy balance closure. *Meteorologische Zeitschrift* 15:597–609.
50. Finkelstein PL, Sims PF (2001) Sampling error in eddy correlation flux measurements. *J Geophys Res Atmos* 106(D4):3503–3509.
51. Papale D, et al. (2006) Towards a standardized processing of net ecosystem exchange measured with eddy covariance technique: Algorithms and uncertainty estimation. *Biogeosciences* 3(4):571–583.
52. Hollinger DY, Richardson AD (2005) Uncertainty in eddy covariance measurements and its application to physiological models. *Tree Physiol* 25(7):873–885.
53. Dragoni D, Schmid HP, Grimmond CSB, Loescher HW (2007) Uncertainty of annual net ecosystem productivity estimated using eddy covariance flux measurements. *J Geophys Res Atmos* 112(D17).
54. Papale D, Valentini R (2003) A new assessment of European forests carbon exchanges by eddy fluxes and artificial neural network spatialization. *Glob Change Biol* 9(4): 525–535.
55. Dengel S, et al. (2013) Testing the applicability of neural networks as a gap-filling method using CH_4 flux data from high latitude wetlands. *Biogeosciences* 10(12):8185–8200.
56. Whalen SC, Reeburgh WS (1992) Interannual variations in tundra methane emission: A 4-year time series at fixed sites. *Global Biogeochem Cycles* 6(2):139–159.
57. Gioli B, et al. (2004) Comparison between tower and aircraft-based eddy covariance fluxes in five European regions. *Agric For Meteorol* 127(1–2):1–16.
58. Karion A, et al. (2013) Long-term greenhouse gas measurements from aircraft. *Atmos Meas Tech* 6(3):511–526.
59. Henderson JM, et al. (2015) Atmospheric transport simulations in support of the Carbon in Arctic Reservoirs Vulnerability Experiment (CARVE). *Atmos Chem Phys* 15(8):4093–4116.
60. Nakagawa S, Schielzeth H (2013) A general and simple method for obtaining R^2 from generalized linear mixed-effects models. *Methods Ecol Evol* 4(2):133–142.
61. Johnson PCD (2014) Extension Nakagawa & Schielzeth's R_GLMM^2 to random slopes models. *Methods Ecol Evol* 5:944–946.
62. Du J, et al. (2014) Inter-calibration of satellite passive microwave land observations from AMSR-E and AMSR2 using overlapping FY3B-MWRI sensor measurements. *Remote Sens* 6:8594–8616.
63. Watts JD, Kimball JS, Bartsch A, McDonald KC (2014) Surface water inundation in the boreal-Arctic: Potential impacts on regional methane emissions. *Environ Res Lett* 9(7):1–13.
64. York D, Evensen NM, Martínez ML, De Basabe Delgado J (2004) Unified equations for the slope, intercept, and standard errors of the best straight line. *Am J Phys* 72(3): 367–375.

Downloaded from https://www.pnas.org by 72.197.169.76 on April 1, 2022 from IP address 72.197.169.76.